

Light curves of tidal disruption events in active galactic nuclei

Chi-Ho Chan^{1,2}, Tsvi Piran¹, and Julian H. Krolik³

¹Racah Institute of Physics, Hebrew University of Jerusalem, Jerusalem 91904, Israel

²School of Physics and Astronomy, Tel Aviv University, Tel Aviv 69978, Israel

³Department of Physics and Astronomy, Johns Hopkins University, Baltimore, MD 21218, USA

April 13, 2020

ABSTRACT

The black hole of an active galactic nucleus is encircled by an accretion disk. The surface density of the disk is always too low to affect the tidal disruption of a star, but it can be high enough that a vigorous interaction results when the debris stream returns to pericenter and punches through the disk. Shocks excited in the disk dissipate the kinetic energy of the disk interior to the impact point and expedite inflow toward the black hole. Radiatively efficient disks with luminosity $\gtrsim 10^{-3}$ Eddington have high enough surface density that the initial stream–disk interaction leads to energy dissipation at a super-Eddington rate. Because of the rapid inflow, only part of this dissipated energy emerges as radiation, while the rest is advected into the black hole. Dissipation, inflow, and cooling balance to keep the bolometric luminosity at an Eddington-level plateau that lasts tens of days. After the plateau, the luminosity decreases in proportion to the disk surface density, with a power-law index between -3 and -2 at earlier times, and possibly a steeper index at later times.

Key words: galaxies: nuclei – accretion, accretion disks – black hole physics – hydrodynamics

1. INTRODUCTION

When a star of mass M_\star and radius r_\star approaches a black hole of mass M_h on an orbit whose pericenter r_p is comparable or smaller than the tidal radius $r_t \equiv r_\star (M_\star/M_h)^{-1/3}$ (Hills 1975), the tidal gravity of the black hole rips the star asunder (e.g., Rees 1988), leading to a tidal disruption event (TDE). The disruption takes place very close to the black hole: in units of the gravitational radius $r_g \equiv GM_h/c^2$, the tidal radius is

$$r_t \approx 50 r_g \left(\frac{M_h}{10^6 M_\odot} \right)^{-2/3} \left(\frac{M_\star}{M_\odot} \right)^{-1/3} \left(\frac{r_\star}{r_\odot} \right). \quad (1)$$

The mass return time, determined by the specific energy of the most bound debris, is the timescale on which this part of the debris returns to pericenter:

$$t_{\text{mb}} \sim 40 \text{ d} \left(\frac{M_h}{10^6 M_\odot} \right)^{1/2} \left(\frac{M_\star}{M_\odot} \right)^{-1/2} \left(\frac{r_p}{r_t} \right)^{3/2}. \quad (2)$$

General relativistic simulations of TDEs starting from stars with realistic structures reveal that these quantities are accurate only within a factor of ~ 2 (Ryu et al. 2020).

The black hole of an AGN is girdled by an accretion disk. When a TDE happens in the vicinity of such a black hole, the passage of the star through the disk leaves the disk largely intact, and the disruption proceeds as if the disk were absent. However, upon return to the vicinity of the black hole, the debris of the disrupted star, being much more extended and dilute than the star, can interact with the disk in a more interesting way (Kochanek 1994; see also Kathirgamaraju et al. 2017).

As we shall argue later, the stream typically has much more inertia than the disk, so it acts as an immovable obstacle to disk rotation. Shocks form where the disk runs into the stream, and the shocks dissipate disk kinetic energy. When the disk surface

density is large enough, the dissipation rate can be highly super-Eddington. This sort of shock dissipation could serve as the energy source for a bright flare different from the energy sources in ordinary TDEs, namely, accretion of any rapidly circularized debris (e.g., Rees 1988) and shocks due to stream self-interaction (Piran et al. 2015).

In Chan et al. (2019), we performed the first hydrodynamics simulations of the collision between the debris stream of a TDE and the pre-existing accretion disk of an AGN. We found that, as long as the stream is much heavier than the disk, our simulation results are sensitive only to how dense the disk is, not how dense the stream is. This observation allows us to extrapolate our simulation results to even heavier streams and make quantitative predictions, even though our simulations did not explicitly cover that regime.

We begin by highlighting the most salient simulation results in §2. Based on these results, we estimate in §3 the bolometric light curve expected when a debris stream tears through the disk. In §4, we scrutinize the dependence of the light curve on black hole mass and disk properties, and we present sample light curves. This discussion is followed by a comparison with previous theoretical models and observations in §5. We end with our conclusions in §6.

2. SUMMARY OF SIMULATIONS

In Chan et al. (2019), we conducted a suite of simulations to investigate the collision between the debris stream of a TDE and the pre-existing accretion disk of an AGN. A snapshot from one of the simulations is displayed in Figure 1. A parabolic stream, representing the returning debris, is injected from the top boundary; the stream strikes the disk the moment it reaches pericenter. Although the simulations considered a specific stream orientation with respect to the disk, the results should be generally

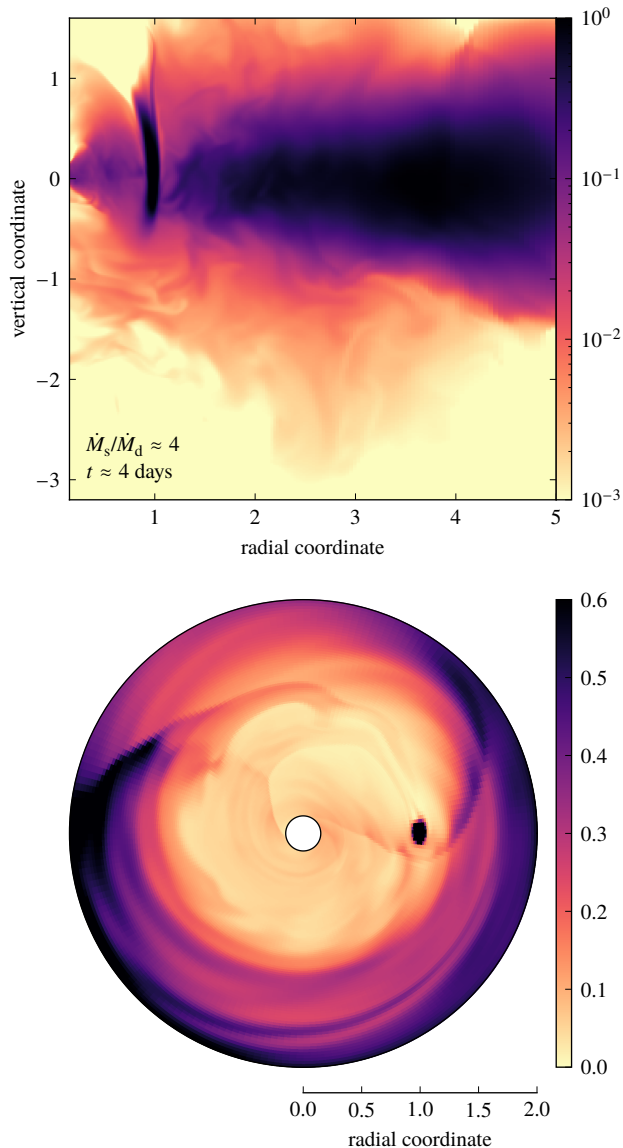


Figure 1. Density snapshot of one simulation in Chan et al. (2019). The top panel is a poloidal slice through the stream impact point with colors in logarithmic scale. The pericenter part of the stream, visible as a vertical structure, penetrates the disk with little difficulty, and energy dissipation makes the disk around the stream geometrically thick. The bottom panel is a midplane slice with colors in linear scale. The dark dot is a section of the stream, and spiral shocks are discernible interior to the stream. The density unit is arbitrary.

applicable to other orientations because a randomly oriented, highly eccentric stream is more likely to cross the disk near pericenter than near apocenter. To better understand disk behavior at late times, we extended every simulation in the suite to twice the duration reported in Chan et al. (2019). These longer durations are still a fraction of t_{mb} , so it is reasonable to keep the stream injection conditions constant.

We adopt as fiducial parameters $M_\star = M_\odot$, $r_\star = r_\odot$, and $r_p = r_t$. The disk dynamical time at the impact point is independent of M_h because it is equal to the stellar dynamical time by definition.

The disk orbital time at the impact point is 2π times that, or

$$t_{\text{orb}} = 2\pi \left(\frac{r_p^3}{GM_h} \right)^{1/2} = 2\pi \left(\frac{r_\star^3}{GM_\star} \right)^{1/2} \approx 3 \text{ h}. \quad (3)$$

Because t_{orb} is the simulation time unit, we can express simulated time in physical units in a way that is valid for all M_h .

The most important parameter governing the collision is \dot{M}_s/\dot{M}_d , the ratio of the mass current of the stream to the mass current of the disk rotating under the stream footprint. We shall see in §4 that $\dot{M}_s/\dot{M}_d \gtrsim 1$ typically; in other words, the stream has too much inertia to be affected by the disk, and it obstructs the rotating disk instead.

The disk interior to the stream impact point is more drastically modified by the collision than the disk exterior to it. The collision excites multiple spiral shocks that span the entire radial extent of the inner disk. The shocks remove angular momentum from the disk gas and transform its kinetic energy into internal energy. Both are so efficient that the disk gas falls from the impact radius to the black hole within a very short inflow time t_{infl} . The top-left panel of Figure 2 tells us that t_{infl} for $\dot{M}_s/\dot{M}_d \gtrsim 0.4$ gradually declines over the course of the event, from ~ 1 d at the start to ~ 0.4 d at $\gtrsim 10$ d. We denote by Σ the disk surface density at the impact point, measured from the midplane to infinity. As evidenced by the top-center panel, the inner disk is speedily depleted in such a way that Σ stays proportional to the disk mass interior to the impact point.

As impact with the disk shaves off part of the stream, the inner disk mass is partially replenished with stream material and Σ diminishes on a timescale $\gg t_{\text{infl}}$. The top-right panel of Figure 2 shows how the decrease of Σ over time steepens gradually: it reaches $\gamma \equiv d \ln \Sigma / d \ln t \sim -3$ at the end of the simulations and may become even steeper afterward. We emphasize that the time-evolution of Σ is due to mechanisms wholly unrelated to those determining the power-law decay of the mass return rate at $t \gtrsim t_{\text{mb}}$. Although $\Sigma(t)$ is not strictly a power law, for the sole purpose of analytic calculations in the following sections, we approximate it as

$$\Sigma/\Sigma_0 \sim 0.1 [t/(10 \text{ d})]^{\bar{\gamma}} \quad \text{for } t \gtrsim 10 \text{ d} \quad (4)$$

and for any \dot{M}_s/\dot{M}_d , where $\bar{\gamma} = -2.5$ and, as below, the subscript zero denotes the value of a quantity shortly after the stream makes contact with the disk.

The dissipated energy heats up the inner disk. As portrayed in the bottom-left panel of Figure 2, heating raises the disk aspect ratio at the impact point to $H/r_p \sim \frac{1}{2}$. The opacity of the hot inner disk is dominated by electron scattering. The cooling time t_{cool} is the time the inner disk takes to release its internal energy as radiation, including the time needed to convert internal energy to radiation, and the time needed for radiation to escape through free streaming, diffusion, or vertical advection due to convection and magnetic buoyancy. The diffusion time is $\sim \tau H/c$, where $\tau = \Sigma \kappa_T$ is the Thomson optical depth and κ_T is the cross section per mass for Thomson scattering. The diffusion time is long because τ drops rather slowly while $H/r_p \lesssim 1$ is much larger than in the unperturbed disk; in fact, the diffusion time is typically $\gtrsim t_{\text{infl}}$ at early times. The cooling time could be even longer because it also takes into account the radiation time. This means most of the radiation is trapped in the inflow toward the black hole and only a small fraction escapes.

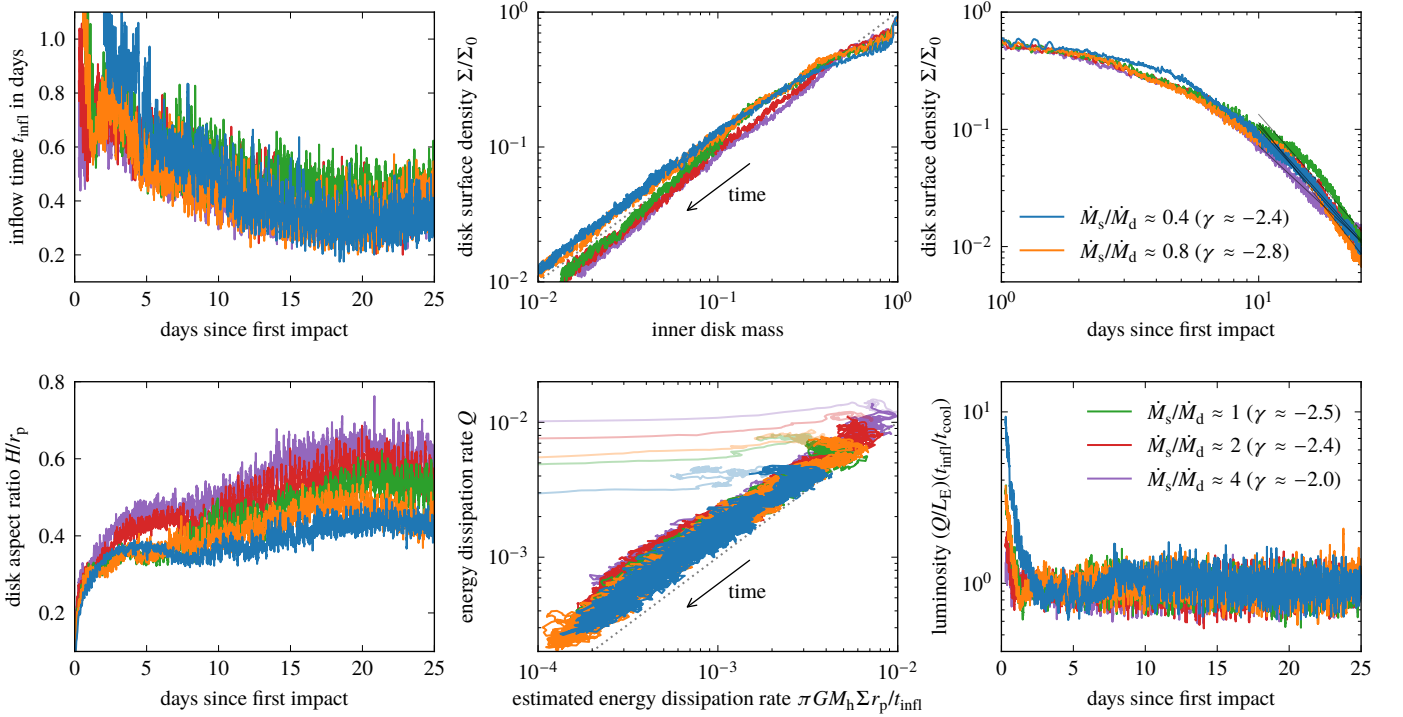


Figure 2. Diagnostics of the simulations in Chan et al. (2019). The legend in the right column applies to all panels. The top-left panel shows the inflow time. The top-center panel shows the correlation between the inner disk mass and the disk surface density Σ at the impact point, both normalized to their initial values; the dotted line marks a one-to-one ratio. The top-right panel shows Σ as a fraction of its initial value; the thin lines are power-law fits to late-time behavior and γ in the legend is the power-law index. The bottom-left panel shows the disk aspect ratio at the impact point. The bottom-center panel compares the energy dissipation rate estimated with Equation (7) and that measured directly from the simulations, both in arbitrary units; early-time data are plotted in a lighter color to highlight the late-time trend, and the dotted line marks a one-to-one ratio. The bottom-right panel shows the bolometric luminosity estimated with Equation (5) as a fraction of the Eddington luminosity; here we assume $t_{\text{infl}}/t_{\text{cool}} \lesssim 1$, which likely holds at early times when Σ is still relatively large.

As discussed at greater length in Chan et al. (2019), a sizable fraction of the stream drills through the disk, the exact fraction being a function of time and \dot{M}_s/\dot{M}_d . The collision imparts a spread of mechanical energy to the stream, such that roughly half of it is gravitationally unbound. Different parts of the stream are put on different trajectories; as a result, the stream fans out into a dilute plume on the other side.

3. ESTIMATION OF BOLOMETRIC LUMINOSITY

The swift inflow in the perturbed inner disk could produce a flare. Similar to a steady-state disk, the energy of the flare ultimately comes from the release of the gravitational energy of the disk gas. The contrast with a steady-state disk is twofold: first, dissipation and inflow happen on much shorter timescales; second, mass resupply from the stream allows more energy to be released than the gravitational energy possessed by the unperturbed disk.

We proposed in Chan et al. (2019) a crude estimate for the bolometric luminosity $L_c(t)$ of the collision-induced flare. Here we use the modified form

$$L_c \sim Q \min(1, t_{\text{infl}}/t_{\text{cool}}), \quad (5)$$

where $Q(t)$ is the energy dissipation rate, while $t_{\text{infl}}(t)$ and $t_{\text{cool}}(t)$ were defined in §2. This equation encapsulates a competition between the inner disk releasing its internal energy as radiation, represented by t_{cool} , and the inflow sweeping this radiation into the black hole, represented by t_{infl} . When $t_{\text{infl}}/t_{\text{cool}} \lesssim 1$, the ratio

$t_{\text{infl}}/t_{\text{cool}}$ estimates the fraction of dissipated energy the inner disk manages to radiate away; when $t_{\text{infl}}/t_{\text{cool}} \gtrsim 1$, all the dissipated energy is radiated away before the gas is accreted, so $L_c \sim Q$. Equation (5) is only an estimate; the true luminosity must be determined by performing time-dependent radiative transfer on the actual distribution of heating and opacity.

The top-left panel of Figure 2 and Equation (3) together tell us that

$$t_{\text{infl}} \sim 4t_{\text{orb}}. \quad (6)$$

Gas does not plunge into the black hole; rather, it spirals inward along trajectories that shift from quasi-circular near the impact radius to more eccentric at smaller radii. When disk material strikes the obstacle posed by the stream, it loses a large part of both its angular momentum and its energy; when it is deflected by shocks at smaller radii, the fractional loss of angular momentum is greater. For this reason, the heating rate as a function of time is reasonably estimated by the orbital kinetic energy of gas orbiting at the impact radius per inflow time:

$$Q \sim \frac{\pi GM_h \Sigma r_p}{t_{\text{infl}}} \sim \frac{\tau}{8\pi} \left(\frac{r_p}{r_g}\right)^{-1/2} \frac{t_{\text{orb}}}{t_{\text{infl}}} L_E, \quad (7)$$

where $L_E = 4\pi GM_h c/\kappa_T$ is the Eddington luminosity. The bottom-center panel of Figure 2 demonstrates that, apart from an initial adjustment phase, this estimate is accurate to within a factor of ~ 2 .

In estimating t_{cool} , we ignore the contributions of radiation time and vertical advection for simplicity. In fact, finite radiation

time slows cooling while vertical advection speeds it, hence the two effects partially cancel. The inner disk starts out optically thick, so

$$t_{\text{cool}} \sim \frac{\tau H}{c} \sim \frac{\tau}{4\pi} \left(\frac{r_p}{r_g}\right)^{-1/2} t_{\text{orb}}, \quad (8)$$

where we used $H/r_p \sim \frac{1}{2}$ in the second step. The inner disk eventually becomes so depleted that $\tau \lesssim 1$ and radiation can escape freely, at which point $L_c \sim Q$. This free-streaming limit is reached only when $t_{\text{inff}}/t_{\text{cool}} \gtrsim 1$, since $t_{\text{inff}} \gtrsim t_{\text{orb}}$ always and $t_{\text{cool}} \lesssim t_{\text{orb}}$ in this limit. Considering that L_c is capped by the minimum function in Equation (5) long before the free-streaming limit kicks in, the limit is irrelevant and we can use Equation (8) for all τ .

We see from Equation (8) that, as long as the inner disk maintains a high enough Σ to make

$$\tau \gtrsim \pi \left(\frac{r_p}{r_g}\right)^{1/2} \frac{t_{\text{inff}}}{t_{\text{orb}}}, \quad (9)$$

we have $t_{\text{inff}}/t_{\text{cool}} \lesssim 1$. Combining Equations (5), (7), and (8) in this regime yields

$$L_c/L_E \sim \frac{1}{2}. \quad (10)$$

This is our main result: The bolometric light curve of a TDE in an AGN starts off with an Eddington-level plateau. Our simulations confirm the validity of Equation (10): $Q t_{\text{inff}}/t_{\text{cool}}$ in the bottom-right panel of Figure 2 quickly stabilizes to $\sim L_E$. The remarkable constancy of L_c is due to the cancellation of t_{inff} and τ in the derivation of Equation (10). When the inner disk is cleared out to the point that Equation (9) is violated and $t_{\text{inff}}/t_{\text{cool}} \gtrsim 1$, the luminosity falls as $L_c \sim Q \propto \Sigma$. Both the plateau duration and the post-plateau L_c depend on the time evolution of a single parameter, Σ .

Because the stream feeds the inner disk, the plateau duration is not limited by the initial inner disk mass and can be $\gg t_{\text{inff}}$; the plateau duration will be estimated in §4. A plateau may not appear if radiation time, convection, or magnetic buoyancy modifies the functional form of t_{cool} .

Our calculations give us only a crude estimate of the bolometric luminosity in some time-averaged sense. Accurate predictions of the light curve and the spectrum should be based on detailed radiation magnetohydrodynamics (MHD) simulations including both free-free and Compton processes as well as the influence of radiation pressure on inner disk structure. The radiative transfer problem is fully three-dimensional on account of the high degree of asymmetry due to the stream arching above the disk, and due to localized shocks and uneven gas heating within the inner disk.

4. LIGHT CURVES

We consider two disk models for the unperturbed disk, depending on how the unperturbed accretion rate $\dot{M}_a \equiv L_a/(\eta c^2)$ compares with the Eddington accretion rate $\dot{M}_E \equiv L_E/(\eta c^2)$, where $\eta = 0.1$ is the fiducial radiative efficiency of a radiatively efficient disk. Any time-steady disk satisfies $\dot{M}_a \sim 4\pi r_p \Sigma_0 v_R$, where v_R is the unperturbed radial velocity; therefore, a choice of disk model boils down to a choice of v_R . The inflow mechanism in the unperturbed disk is the outward transport of angular momentum

by internal stresses, but once the stream strikes the disk, inflow is driven by spiral shocks instead.

If $\dot{M}_a/\dot{M}_E \gtrsim 10^{-3}$, we assume the disk is geometrically thin, optically thick, and radiatively efficient (Shakura & Sunyaev 1973) with fiducial stress parameter $\alpha = 0.1$. Both the disk aspect ratio and v_R/v_ϕ at the impact point are $\ll 1$ in this model; here v_ϕ is the orbital velocity. As a result, Σ_0 is large, and the initial energy dissipation rate Q_0 , given by Equation (7), is large as well.

If \dot{M}_a is any lower, the disk could be a geometrically thick, optically thin, radiatively inefficient accretion flow (RIAF) (e.g., Ichimaru 1977; Rees et al. 1982; Narayan & Yi 1994). Parameterizing the radial velocity in a geometrically thick disk as $v_R \sim \alpha' v_\phi$, we can write

$$\kappa_T \Sigma_0 \sim \frac{2}{\alpha' \eta'} \frac{L_a/L_E}{(r_p/r_g)^{1/2}}. \quad (11)$$

The factor of two on the right-hand side is included so that the equation matches the form of its radiatively efficient counterpart. We emphasize that α' is merely a parameterization; for simplicity we take $\alpha' = 0.1$. Ryan et al. (2017) performed general relativistic MHD simulations of RIAFs assuming that electrons are heated by Coulomb scattering off ions at a rate derived empirically from solar wind measurements (Ressler et al. 2015). They found that the effective radiative efficiency is $\eta' \sim 10^{-2}$ for $\dot{M}_a/\dot{M}_E \sim 10^{-5}$, suggesting that accretion may proceed at efficiencies close to radiatively efficient values even at very low accretion rates. We adopt this value of η' below. The much larger v_R/v_ϕ in a RIAF compared to a radiatively efficient disk means that Σ_0 and hence Q_0 are much smaller.

The top panel of Figure 3 displays Q_0 for a radiatively efficient disk, and Figure 4 does the same for a RIAF. We end Figure 3 at $\dot{M}_a/\dot{M}_E = L_a/L_E = 10^{-4}$ and begin Figure 4 at $\dot{M}_a/\dot{M}_E = (\eta/\eta')(L_a/L_E) = 10^{-2}$ in view of the uncertain \dot{M}_a/\dot{M}_E marking the transition between the two disk models. Because $Q_0 \gtrsim L_E$ generally in a radiatively efficient disk, there is enough dissipation to power Eddington-level luminosity. By contrast, v_R is much larger and Σ_0 much smaller in a RIAF with the same \dot{M}_a , so $Q_0 \ll L_E$. A noticeable flare is unlikely, so we drop the RIAF from further consideration.

The middle panel of Figure 3 plots the initial value of $t_{\text{inff}}/t_{\text{cool}}$ for the radiatively efficient disk, with t_{inff} and t_{cool} from Equations (6) and (8) respectively. For most of the parameter space plotted, $t_{\text{inff}}/t_{\text{cool}} \lesssim 1$, so $L_c \sim \frac{1}{2} L_E$ irrespective of M_h and L_a/L_E . With the gradual depletion of the inner disk, $t_{\text{inff}}/t_{\text{cool}} \propto 1/\Sigma$ rises but $Q \propto \Sigma/t_{\text{inff}}$ falls, and the two changes offset each other to sustain a constant L_c . The luminosity plateau continues until $t_{\text{inff}}/t_{\text{cool}} \sim 1$. The plateau duration is calculated assuming that Σ follows Equation (4); if $t_{\text{inff}}/t_{\text{cool}} \lesssim 0.1$ initially, Equation (4) allows us to determine only an upper limit of $\lesssim 10$ d to the plateau duration. The plateau duration is shown in the bottom panel, and explicit expressions can be found in Appendix A. The plateau typically lasts tens of days. After the plateau, the inner disk fades as $L_c \sim Q \propto \Sigma$. For a small part of the parameter space, $t_{\text{inff}}/t_{\text{cool}} \gtrsim 1$ even at the beginning; these inner disks do not have a luminosity plateau.

The plateau duration is comparable to but typically smaller than t_{mb} . Although the stream mass current decreases during the plateau, the disk mass current would decrease by an even greater amount, according to Equation (4). Therefore, the stream would

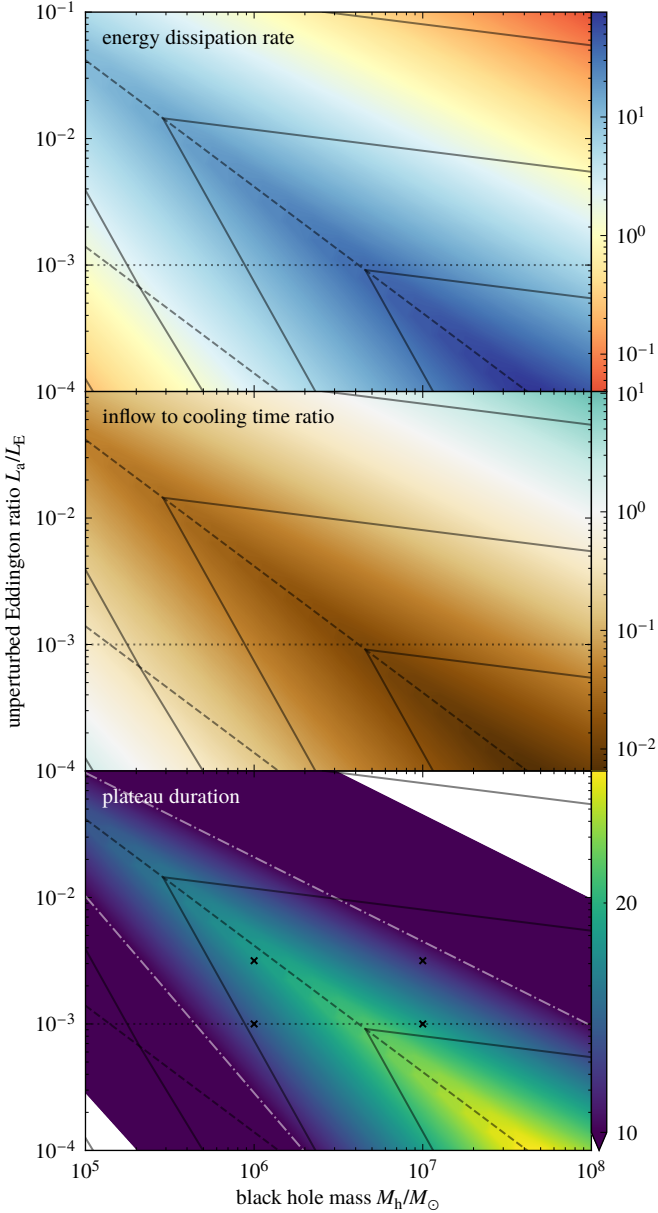


Figure 3. Color contours of three properties of the perturbed inner disk, as functions of the black hole mass M_h and the Eddington ratio L_a/L_E of the unperturbed disk, with other parameters fixed at their fiducial values. This figure portrays the case in which the unperturbed inner disk is a radiatively efficient disk, while Figure 4 illustrates the case of a RIAF. The top panel shows the initial energy dissipation rate Q_0 divided by the Eddington luminosity L_E . The middle panel shows the initial value of the ratio of inflow to cooling time $t_{\text{infl}}/t_{\text{cool}}$. The bottom panel shows the plateau duration in units of days; in the white parts there is no plateau, while in the blue parts outside the dash-dotted lines the plateau duration is ≤ 10 d. The crosses are the values of $(M_h, L_a/L_E)$ for which light curves are shown in Figure 5. In all panels, the lower dashed line at $L_a \sim 1.8 \times 10^{40}$ erg s $^{-1}$ separates two opacity regimes of the unperturbed disk: opacity is dominated by free-free absorption below and electron scattering above. The upper dashed line at $L_a \sim 5 \times 10^{41}$ erg s $^{-1}$ separates two pressure regimes of the unperturbed disk: pressure is dominated by gas below and radiation above. The three gray, chevron-shaped contours are drawn, from bottom-right to top-left, where the unperturbed M_s/M_d is 1, 10, and 100 respectively. The horizontal dotted line marks the value of L_a/L_E below which the disk may become a RIAF.

become heavier and heavier relative to the disk as the event progresses, so the assumption that disk dissipation dominates

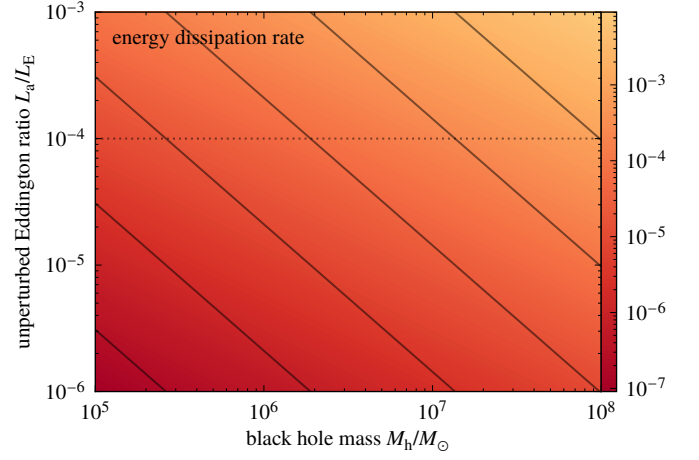


Figure 4. Color contours of the initial energy dissipation rate Q_0 divided by the Eddington luminosity L_E , as functions of the black hole mass M_h and the Eddington ratio L_a/L_E of the unperturbed disk, with other parameters fixed at their fiducial values. This figure portrays the case in which the unperturbed inner disk is a RIAF, while Figure 3 illustrates the case of a radiatively efficient disk. Gray contours are drawn at constant levels of unperturbed M_s/M_d , starting from 10^4 in the top-right and increasing by a factor of 10 for each contour toward the bottom-left. The horizontal dotted line marks the value of L_a/L_E above which the RIAF may become a radiatively efficient disk.

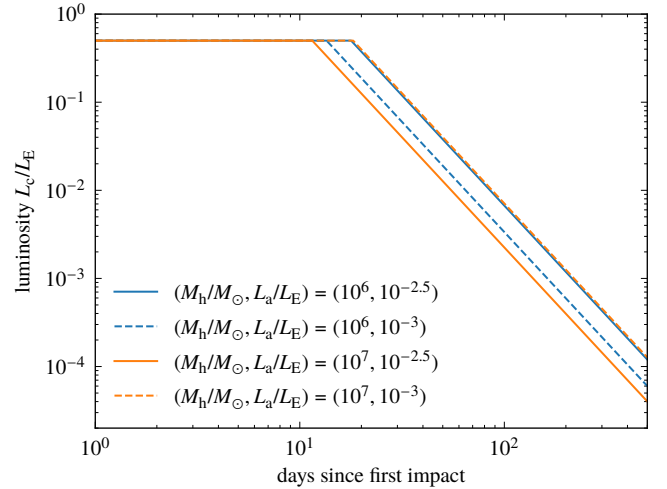


Figure 5. Estimated bolometric light curves assuming that the unperturbed disk is radiatively efficient. The choices of $(M_h/M_\odot, L_a/L_E)$ are marked with crosses in the bottom panel of Figure 3. The level of the initial plateau is given by Equation (10).

remains valid.

Figure 5 displays the estimated bolometric light curves for four radiatively efficient unperturbed disks. For all four, the luminosity plateau lasts ~ 20 d to within a factor of ~ 1.5 . After the plateau, $L_c \sim Q \propto \Sigma \propto t^{\tilde{\gamma}}$. The power-law index of the falloff is steeper than $-\frac{5}{3}$, the power-law index of the mass return rate (Phinney 1989), and the two are completely unrelated.

The stream exits the impact point with a distribution of mechanical energy. The gravitationally bound part of the outgoing material eventually falls back onto the disk at larger distances, colliding inelastically because the disk is much denser. The luminosity enhancement due to this energy dissipation is not

included in Figure 5; its characterization is left to future work.

5. DISCUSSION

The Eddington-level luminosity plateau discussed here is qualitatively different from the plateaus in other TDE models.

The classical picture (e.g., Rees 1988) describes a TDE around an isolated black hole. The debris, returning to pericenter at super-Eddington rates for up to several years (e.g., Evans & Kochanek 1989), quickly forms a circular disk. The disk bolometric luminosity tracks the mass return rate, but instead of going super-Eddington, it reaches a plateau (e.g., Loeb & Ulmer 1997; Krolik & Piran 2012). It should be noted that the classical picture has been called into question by simulations (Shiokawa et al. 2015) and their implications for observations (Piran et al. 2015; Krolik et al. 2020). In particular, the predicted plateau is not seen in the light curves of most optical TDEs (van Velzen et al. 2020), and its existence is under debate.

The disk dissipation mechanism we discussed applies to a TDE around a black hole with a pre-existing accretion disk. In contrast with the classical picture, the plateau is produced when the debris slams into the disk, and the principal parameter determining whether and for how long our plateau can be observed is the accretion rate of the unperturbed disk. Moreover, the plateau is shorter than in the classical picture, lasting only tens of days. One respect in which our mechanism does resemble the classical picture, however, is that the plateaus in both cases arise from radiation trapping, that is, a situation in which inflow is faster than radiation can escape by diffusion.

A handful of TDEs have been observed to have luminosity plateaus. Saxton et al. (2019) reported a TDE candidate in a quiescent galaxy with a $\sim 10^7 M_\odot$ black hole. The 0.2-to-2 keV flux held steady for ~ 90 d at $\sim 10^{-3}$ Eddington levels before diminishing as a power law. The plateau duration is ~ 3 times the longest plateau duration our disk dissipation mechanism may produce. However, given the many simplifications we made in our estimates, it remains possible that this soft X-ray plateau was powered by disk dissipation. More recently, Liu et al. (2020) found an ultraviolet plateau in a TDE occurring in an AGN.

Our simulations did not account for magnetic fields. Magnetic field loops in the outer disk can protrude into the depleted inner disk (Noble et al. 2011), enhancing magnetic stresses to the degree that the outer disk may replenish the inner disk on a timescale as fast as a few days. Any resupply from the outer disk complements resupply from the stream, keeping Σ at a high level and prolonging the plateau.

Our calculations do not capture the gradual increase of the stream mass current to its peak value in realistic TDEs. During the early parts of this rising phase when the stream is lighter than the disk, our predictions here do not apply, but shocks excited by the light stream can send disk material toward the black hole. Therefore, at later times when the stream is heavier than the disk and our predictions do apply, the disk will have a surface density smaller than its unperturbed value, suggesting that any luminosity plateau that may appear would be shorter. However, if the net mass loss from the inner disk during the rising phase is small due to resupply from the stream or the outer disk, the plateau might be extended. Exactly how a time-varying stream mass current affects the light curve is the subject of future simulations.

6. CONCLUSIONS

The black hole of an AGN is surrounded by an accretion disk. The debris stream of a TDE around such a black hole runs into the disk near pericenter. The stream delivers a much stronger mass current to the impact point than the disk does, so the dynamical evolution of the former is largely unaffected by the latter. On the other hand, the heavy stream prevents the disk from rotating freely. Shocks are formed where the disk smashes into the stream; disk gas is deflected inward and drives shocks against gas closer in. As a result, the kinetic energy of the disk interior to the impact point is dissipated into internal energy at a rate high enough to power a bright flare.

If the unperturbed disk is radiatively efficient, that is, if its luminosity is $\geq 10^{-3}$ Eddington, then the disk surface density Σ is large enough to make the initial energy dissipation rate $Q \propto \Sigma$ super-Eddington. Conversely, if the unperturbed disk is a RIAF, Σ is too small and Q too low to beget any visible flare.

Because gas in the inner disk falls into the black hole in only a few orbits, not all the energy dissipated issues forth as radiation. We estimate the bolometric luminosity as $L_c \sim Q \min(1, t_{\text{infl}}/t_{\text{cool}})$, where t_{infl} is the time for a gas packet to flow inward from the impact point to the black hole, and t_{cool} is the cooling time of the inner disk. The luminosity at early times is regulated to an Eddington-level plateau by the facts that $Q \propto \Sigma/t_{\text{infl}}$ and $t_{\text{cool}} \propto \Sigma$.

The luminosity plateau ends when $t_{\text{infl}}/t_{\text{cool}}$ falls to ~ 1 , which occurs after the disk has been depleted by shock-driven inflows. Resupply from the stream and the outer disk could keep both Σ and t_{cool} large, delaying the end of the plateau. If only stream resupply acts, as in our simulations, the plateau duration is of order tens of days. Following the end of the plateau, $L_c \propto \Sigma$, which in our simulations declines as a power law in time with index between -3 and -2 at earlier times, and possibly a steeper index at later times.

After striking the disk, the stream is dispersed and leaves the impact point with a wide range of mechanical energy; hence, it has a much lower density than before. The gravitationally bound part of this material collides inelastically with the disk at larger distances; the boost to late-time emission from the dissipated energy will be explored in future work.

The authors thank Kojiro Kawana for the question that prompted this investigation and Tatsuya Matsumoto for fruitful discussions. This work was partially supported by ERC advanced grant ‘‘TRex’’ (CHC and TP) and NSF grant AST-1715032 (JHK).

APPENDIX

A. PLATEAU DURATION

We present explicit expressions for the plateau duration when the unperturbed disk is radiatively efficient (Shakura & Sunyaev 1973). If the unperturbed disk is dominated by gas pressure and Thomson scattering opacity, the plateau duration is

$$\sim 24 \text{ d} \left[\left(\frac{M_h}{10^6 M_\odot} \right)^{14/15} \left(\frac{M_\star}{M_\odot} \right)^{11/30} \left(\frac{r_\star}{r_\odot} \frac{r_p}{r_t} \right)^{-11/10} \times \left(\frac{L_a/L_E}{10^{-3}} \right)^{3/5} \left(\frac{\alpha}{0.1} \right)^{-4/5} \left(\frac{\eta}{0.1} \right)^{-3/5} \right]^{-1/\bar{\gamma}}, \quad (\text{A1})$$

where $\bar{\gamma} = -2.5$ from Equation (4). If the unperturbed disk is dominated instead by radiation pressure and Thomson scattering opacity, the plateau duration is

$$\sim 32 \text{ d} \left[\left(\frac{M_{\text{h}}}{10^7 M_{\odot}} \right)^{-2/3} \left(\frac{M_{\star}}{M_{\odot}} \right)^{-1/3} \left(\frac{r_{\star}}{r_{\odot}} \frac{r_{\text{p}}}{r_{\text{t}}} \right) \times \left(\frac{L_{\text{a}}/L_{\text{E}}}{10^{-3}} \right)^{-1} \left(\frac{\alpha}{0.1} \right)^{-1} \left(\frac{\eta}{0.1} \right) \right]^{-1/\bar{\gamma}}. \quad (\text{A2})$$

REFERENCES

- Chan, C.-H., Piran, T., Krolik, J. H., & Saban, D. 2019, *ApJ*, **881**, 113
- Evans, C. R. & Kochanek, C. S. 1989, *ApJL*, **346**, L13
- Hills, J. G. 1975, *Natur*, **254**, 295
- Ichimaru, S. 1977, *ApJ*, **214**, 840
- Kathirgamaraju, A., Barniol Duran, R., & Giannios, D. 2017, *MNRAS*, **469**, 314
- Kochanek, C. S. 1994, *ApJ*, **422**, 508
- Krolik, J. H. & Piran, T. 2012, *ApJ*, **749**, 92
- Krolik, J., Piran, T., & Ryu, T. 2020, arXiv: 2001.03234
- Liu, Z., Li, D., Liu, H.-Y., et al. 2020, arXiv: 2004.01517
- Loeb, A. & Ulmer, A. 1997, *ApJ*, **489**, 573
- Narayan, R. & Yi, I. 1994, *ApJL*, **428**, L13
- Noble, S. C., Krolik, J. H., Schnittman, J. D., & Hawley, J. F. 2011, *ApJ*, **743**, 115
- Phinney, E. S. 1989, in Symposium of the International Astronomical Union 136, *The Center of the Galaxy*, ed. M. Morris (Netherlands: Springer), 543
- Piran, T., Svirski, G., Krolik, J., Cheng, R. M., & Shiokawa, H. 2015, *ApJ*, **806**, 164
- Rees, M. J., Begelman, M. C., Blandford, R. D., & Phinney, E. S. 1982, *Natur*, **295**, 17
- Rees, M. J. 1988, *Natur*, **333**, 523
- Ressler, S. M., Tchekhovskoy, A., Quataert, E., Chandra, M., & Gammie, C. F. 2015, *MNRAS*, **454**, 1848
- Ryan, B. R., Ressler, S. M., Dolence, J. C., et al. 2017, *ApJL*, **844**, L24
- Ryu, T., Krolik, J., Piran, T., & Noble, S. C. 2020, arXiv: 2001.03501
- Saxton, R. D., Read, A. M., Komossa, S., et al. 2019, *A&A*, **630**, A98
- Shakura, N. I. & Sunyaev, R. A. 1973, *A&A*, **24**, 337
- Shiokawa, H., Krolik, J. H., Cheng, R. M., Piran, T., & Noble, S. C. 2015, *ApJ*, **804**, 85
- Van Velzen, S., Gezari, S., Hammerstein, E., et al. 2020, arXiv: 2001.01409